Supplementary information

Dynamics of mitochondrial structure, biogenesis and function in skeletal muscle of critically ill patients

Anika Wickert, MD, Julius J. Grunow, MD, Tobias Wollersheim, MD, Lilian Jo Engelhardt, MD, Stefan Groß, PhD, Sara Timm, Matthias Ochs, MD, Jenny Meinhardt, MD, Werner Stenzel, MD, Michael Boschmann, MD, Steffen Weber-Carstens, MD, Jens Fielitz, MD

Table of Contents

Supplementary Methods **2**
Control patients **2**
Muscle biopsy procedure **2**
Transmission electron microscopy **2**
RNA extraction, reverse transcription and qRT-PCR **4**
RNA sequencing and statistical analyses **4**
Protein extraction and Western Blot analysis **5**
Spectrophotometric assay **6**
eTables ***8***
Table e1. Baseline characteristics of control groups **8**
Table e2. Comparison of Mitochondrial Morphology according to SOFA-Score **9**
Table e3. Comparison of Mitochondrial Morphology according to Sepsis Diagnosis **11**
Table e4. Comparison of Mitochondrial Morphology between Day 5 and 15 only including Patients that were investigated on both Days **13**
Table e5. Primer pairs for quantitative RT-PCR **14**
eFigures ***16***
Figure e1. Mitochondrial ultrastructure is disturbed in skeletal muscle of ICU patients. **16**
Figure e2. A dysregulation of mitochondrial genes and transcription factors occurs in muscle of ICU patients. **19**
Figure e3. The content of ETC proteins is reduced in skeletal muscle of ICU patients. **21**
Figure e4. Mitochondrial function is decreased in skeletal muscle of ICU patients. **23**
Figure e5. Volcano plots of differential gene expression in mouse tibialis anterior muscle following CLP-induced sepsis. **26**
Figure e6. Mitochondrial gene expression organized by ETC complex. **27**
Figure e7. Expression of mitochondrial genes contained in ETC complexes I-V in mouse TA muscle after 24 and 96 hours of sepsis. **29**
References ***30***

Supplementary Methods

Control patients

Muscle biopsy specimens from 12 healthy individuals, who were included in a clinical study investigating the effects of exercise, were used as controls for quantitative real-time PCR, spectrophotometric and Western blot analyses. Due to the scarcity of the tissue, only seven of the twelve patients could be included in the spectrophotometric assay. Quantitative real-time PCR for *TFAM* and *NRF1* had already been performed during the initial trial and therefore used a separate cohort of healthy controls (n = 5), as summarized in Table e1 (*TFAM*/*NRF1* Measurements). Stereological evaluation of the transmission electron microscopy images included healthy individuals who underwent a muscle biopsy as part of routine clinical diagnostics (n = 5), where a muscle pathology was initially suspected but ultimately ruled out. Clinical data of controls can be found in Table e1.

Muscle biopsy procedure

A muscle biopsy specimen was obtained under local anesthesia using lidocaine. An incision was made in to expose the *vastus lateralis* muscle. The muscle biopsy specimen was then retrieved. Any bleeding was addressed surgically and the wound was closed with sutures and dressed.

Transmission electron microscopy

The muscle biopsy specimens were processed as detailed in Rathke 2016 (1). Muscle biopsy specimens from critically ill patients were immediately placed in fixative (2.5% glutaraldehyde in 0.1 M cacodylate buffer; Serva, Heidelberg, Germany) at the bedside in the intensive care unit (ICU) for transmission electron microscopy (TEM). The fixed specimens were post-fixed with 1 % osmium tetroxide (Electron Microscopy Sciences, Hatfield, USA) in 0.1 M cacodylate buffer, then dehydrated in a graded ethanol series before being transferred to Epon resin (Roth, Karlsruhe, Germany). Ultrathin sections were cut using an ultramicrotome (Leica, Wetzlar,

Germany) and a diamond knife (Diatome, Nidau, Switzerland). The sections were then collected on pioloform-coated copper grids and finally contrasted with lead citrate (Merck Millipore, Darmstadt, Germany), according to the method described by Reynolds et al. (2)

Muscle biopsy specimens from healthy individuals, retrieved for TEM during routine clinical practice, were transported to the neuropathology department before fixation and further processing. The control samples were processed according to the Department of Neuropathology`s protocol at the Charité - Universitätsmedizin Berlin, as described by Holzer et al. (3).

Grids were examined using a Zeiss Leo 906 electron microscope (Carl Zeiss, Oberkochen, Germany) with an acceleration voltage of 80 kV. Images were recorded using a slow-scan 2K CCD camera (TRS, Moorenweis, Germany).

For the quantitative stereological two-dimensional TEM analysis, the field of view was defined according to the rules of systematic uniform random area sampling (4), using the same ×27.800 magnification on the microscope. The images were then analyzed stereologically using the Stepanizer software (5). A test system of line pairs or points was used. Profiles that were defined as a visible, independent parts of mitochondria were counted, as two profiles might be part of the same mitochondrion. Volume density was calculated by dividing the number of points on the structure by the total number of testing points. The length of the inner mitochondrial membrane was calculated as the surface-to-volume ratio, according to current recommendations (6). The intersections of the inner mitochondrial membrane were divided by the number of points on the structure, which was then multiplied by the length of the test line. This analysis was comparable to that performed by Nielsen et al. (7). The stereological analysis was performed according to a morphological classification of mitochondria as either intact

(intact and distinct membrane structure, no swelling; Figure e1a-c) or disturbed (disrupted membrane structure, with swelling and/or loss of normal cristae organization; Figure e1d-f).

RNA extraction, reverse transcription and qRT-PCR

RNA isolation, reverse transcription and quantitative real-time polymerase chain reaction (qRT-PCR) were performed as previously described (8-10). In brief, the TRIzol® Reagent (Invitrogen AG, CA, USA, CAS 9048-46-8) was used to extract total RNA from muscle tissue according to the manufacturer's protocol. Reverse transcription of 1.2 µg of RNA into complementary DNA (cDNA) was performed using the SuperScript® First-Strand Synthesis System (Invitrogen AG, CA, USA, CAS 9068-38-6) according to the manufacturers protocol. qRT-PCR was performed using SYBR® Green PCR Master Mix (Merck, Germany, CAS 163795-75-3) and self-designed primers (see Table e5 for primer sequences).

RNA sequencing and statistical analyses

Six biological replicates were sequenced for all sample types (WT, sham or CLP, 24 or 96 hours after surgery). Total RNA analyses were performed using an Agilent 2100 Bioanalyzer (Agilent Technologies, Inc., California, USA). Library preparation of 500 ng RNA was performed using the Illumina TruSeq Stranded mRNA Kit. To check integrity, the resulting cDNA was evaluated again using an Agilent 2100 Bioanalyzer. Sequencing was performed using an Illumina HiSeq 4000 sequencer. The initial quality check of the RNA-sequencing results was performed using FASTQC software (v0.11.5; Babraham Bioinformatics, UK; available online at www.bioinformatics.babraham.ac.uk/projects/fastqc). The sequencing reads were mapped to the mouse whole genome (mm10) using the STAR aligner (v2.5.3a; default parameters) (11). Read counts for each gene (Gencode vM12) were extracted from the BAM file using the featureCounts software package (v1.5.1) (12). To avoid background signal noise, genes with fewer than 10 reads across all samples were excluded. Read counts from the different biological

groups were then analyzed for differential expression using the DESeq2 R statistical package (version 1.16.1) (13). The transcriptome data can be found in EBI Annotare v.2.0 (project ID E-MTAB-10960).

Pathway enrichment analysis was performed using the Bioinformatics Resources 6.8 version of the Database for Annotation, Visualization and Integrated Discovery (DAVID) (https://david.ncifcrf.gov), using the BP_ALL output (all biological process terms) (14, 15).

Protein extraction and Western Blot analysis

Protein extraction was performed as previously published (9, 16-18). Briefly, the muscle tissue was minced in homogenization buffer (1:20 w/v, 20 mM Tris, 40 mM KCl, 2 mM EGTA and 250 mM sucrose) at 4°C for 60 seconds at 500 rpm, after which it was cleared by centrifugation (4°C, 600 x g, 10 min). The Bradford assay (Invitrogen AG, CA, USA) was used to determine the protein concentration. Proteins (15 µg) were separated using a 10% sodium dodecyl sulfate polyacrylamide gel electrophoresis (SDS-PAGE) and transferred onto a nitrocellulose membrane (Bio-Rad Laboratories, Inc., CA, USA). The membranes were then blocked with 1% BSA (Sigma-Aldrich, Inc., MO, USA, CAS 9048468) in Tris-buffered saline containing 0.1 % Tween-20 (TBST) at room temperature for one hour. The membranes were then washed and incubated with an OXPHOS antibody cocktail (Invitrogen AG, CA, USA), which contains primary antibodies that detect one protein per electron transport chain (ETC) complex subunit: anti-NDUFB (NADH:ubiquinone oxidoreductase subunit B8) for complex (C) I, anti-SDHB (succinate dehydrogenase complex subunit B) for CII, anti-UQCRC2 (ubiquinol-cytochrome c reductase core protein 2) for CIII, anti-cytochrome c oxidase II subunit for CIV, and anti-ATP5A1 (ATP synthase F1 subunit alpha) for CV. In our skeletal muscle lysates, the CI subunit NDUFB8 was not reliably detectable under the applied conditions; therefore, NDUFB8 immunoblot quantification is not reported. A horseradish peroxidase-conjugated anti-mouse antibody (Cell Signaling Technology, Inc., MA, USA) was used as secondary antibody. The

signals were visualized and detected using the ChemiDoc MP imaging system (Bio-Rad Laboratories, Inc., CA, USA). Glyceraldehyde-3-phosphate dehydrogenase (GAPDH) was used as a loading control.

Spectrophotometric assay

We measured ETC enzyme activity spectrophotometrically following a recently published protocol (11). For these assays, the proteins were diluted in sucrose buffer (0.5 µg/µl) and stored at -80°C until use. The activities of complexes (C) I, CII, CIII, CIV, CI+III, CII+III, and citrate synthase (CS) were measured by spectrophotometric assays according to a recently published protocol (19). Briefly, *CI activity* was measured in a solution containing: potassium phosphate (50 mM, pH 7.5), bovine serum albumin (BSA, 3 mg/ml, CAS 9048-46-8), potassium cyanide (KCN, 300 µM, CAS 151-50-8), reduced nicotinamide adenine dinucleotide (NADH, 100 µM, CAS 58-68-4), ubiquinone (60 µM, CAS 303-98-0), and Tris(hydroxymethyl)aminomethane (Tris,10 mM, pH 7.6, CAS 77-86-1). Absorbance slopes were detected at a wavelength of 340 nm. CI activity was measured for each sample in the presence and absence of the CI inhibitor rotenone (10 µM, CAS 83-79-4), in order to determine rotenone-sensitive and rotenone-insensitive activity. CI activity was determined by subtracting the CI activity measured in the presence of rotenone from the CI activity measured in its absence. *CII activity* was measured in a CII buffer containing: potassium phosphate (25 mM, pH 7.5), BSA (1 mg/ml), KCN (300 µM), succinate (20 mM, CAS 110-15-6), 2,6-dichlorophenolindophenol sodium salt hydrate (DCPIP, 80 µM, CAS 956-48-9), and decylubiquinone (DUB, 50 µM, CAS 55486-00-5). Malonic acid (10 mM, CAS 141-82-2) was used as a CII inhibitor. Absorbance slopes were detected at a wavelength of 600 nm. CII activity was determined by subtracting the CII activity measured in the presence of malonic acid from the CII activity measured in its absence. *CIII* activity was assayed in CIII buffer containing: potassium phosphate (25 mM, pH 7.5), oxidized cytochrome c (Cyt c,75 µM, CAS 9007-43-6), KCN (500 µM), ethylenediaminetetraacetic acid

(EDTA,100 µM, pH 7.5, CAS 6381-92-6), Tween-20 (0.025 %, CAS 9005-64-5), and decylubichinol (DubH2, 100 µM, CAS 64845-31-4). Antimycin A (AMA 10 µg/ml, CAS 1397-94-0) was used as the CIII inhibitor, and changes in absorbance were determined at 550 nm. CIII activity was determined by subtracting the CIII activity measured in the presence of AMA from that measured in the absence of the inhibitor. *CIV activity* was measured in a CIV buffer solution containing potassium phosphate (50 mM, pH 7.0), and reduced cytochrome c (Cyt c H2, 60 µM). Absorbance was measured at 550 nm and the specific inhibitor was KCN (300 µM). CIV activity was determined by subtracting the CIV activity measured in the presence of KCN from the CIV activity measured in its absence. The *combined CI+III assay* was used to detect coenzyme Q deficiency. This was performed in a potassium phosphate buffer (50 mM, pH 7.5) containing BSA (1 mg/ml), KCN (300 µM)), oxidized cytochrome c (50 µM)), and NADH (200µM), measuring the absorbance at 550 nm. Rotenone (10 µM) was used as a CI inhibitor. Calculation of CI+III activity was performed in the same way as for CI. The *combined CII+III assay* was also used to detect coenzyme Q deficiency. This was performed in a potassium phosphate buffer (20 mM, pH 7.5), KCN (300 µM), succinate (10 mM), and oxidized cytochrome c (50 µM). Absorbance was detected as a gradient at 550 nm, and the CIII inhibitor AMA (10 µg/ml) was used to detect the specific activity. CII+III activity was calculated by subtracting the activity measured in the presence and absence of AMA. *Citrate synthase* (CS) activity was used as a quantitative marker for mitochondrial content. This assay was performed in a Tris buffer (100 mM, pH 8.0, CAS 77-86-1), containing Triton-X (0.1%, CAS 9002-93-1), 5,5-dithio-bis(2-nitrobenzoic acid) (DTNB (100 µM, CAS 552-16-9), acetyl-CoA (300 µM, CAS 72-89-9) and oxalacetic acid (10 mM, CAS 328-42-7). Changes in absorbance were determined at 412 nm. The individual ETC activity was normalized either to the amount of tissue used (as an estimate of total enzyme activity in muscle; i.e. tissue enzyme activity) or to the respective CS activity (as an estimate of enzyme activity per mitochondria; i.e. mitochondrial enzyme activity).

eTables

Table e1. Baseline characteristics of control groups

Variable	Electron Microscopy	TFAM / NRF1 Measurements	Molecular Analyses
N	5	5	12
Age, years	32 [26.5 – 33.5]	61 [39 – 66.5]	57.6 ± 2.2
Female, n (%)	3 (60)	2 (40)	0 (0)
BMI, kg/m^2	19.8 [18.8 – 31.0][a]	Not available	34.1 ± 0.9

The data are shown as either count and percentage, median and interquartile range, and mean and standard deviation, respectively.

[a] Because only three values were available, numbers shown depict the median and range.

192 **Table e2. Comparison of Mitochondrial Morphology according to SOFA-Score**

Variable		**SOFA score ≤ 12**	**SOFA score > 12**	**p-value**
Day 5	Profiles of Intact Mitochondria	0.24 [0.18 – 0.34]	0.21 [0.18 – 0.34]	0.802
	Profiles of Disturbed Mitochondria	6.53 [3.85 – 7.52]	4.45 [2.82 – 5.74]	0.159
	Volume Density of Intact Mitochondria	0.35 [0.20 – 0.54]	0.30 [0.19 – 0.48]	0.837
	Volume Density of Disturbed Mitochondria	4.76 [2.72 – 6.47]	4.46 [2.05 – 5.79]	0.837
	Surface-to-Volume Ratio of the Inner Mitochondrial Membrane	0.65 [0.53 – 0.88]	0.71 [0.49 – 0.91]	1.000
Day 15	Profiles of Intact Mitochondria	0.19 [0.15 – 0.33]	0.25 [0.17 – 0.38]	0.740
	Profiles of Disturbed Mitochondria	4.43 [1.51 – 6.36]	5.74 [4.69 – 6.08]	0.364
	Volume Density of Intact Mitochondria	0.30 [0.21 – 0.50]	0.35 [0.23 – 0.65]	0.740
	Volume Density of Disturbed Mitochondria	2.12 [1.26 – 5.65]	4.80 [4.30 – 6.00]	0.133

	Surface-to-Volume Ratio of the Inner Mitochondrial Membrane	0.86 [0.51 – 1.13]	0.91 [0.59 – 0.87]	1.000

193

194

195 **Table e3. Comparison of Mitochondrial Morphology according to Sepsis**
196 **Diagnosis**
197

Variable		**No Sepsis**	**Sepsis**	**p-value**
Day 5	Profiles of Intact Mitochondria	0.25 [0.20 – 0.59]	0.18 [0.12 – 0.33]	0.324
	Profiles of Disturbed Mitochondria	4.59 [2.82 – 6.92]	3.91 [1.45 – 7.07]	0.768
	Volume Density of Intact Mitochondria	0.36 [0.23 – 0.72]	0.41 [0.14 – 0.47]	0.838
	Volume Density of Disturbed Mitochondria	4.10 [1.62 – 5.79]	4.22 [1.51 – 7.63]	0.633
	Surface-to-Volume Ratio of the Inner Mitochondrial Membrane	0.72 [0.56 – 0.97]	0.75 [0.49 – 0.77]	0.874
Day 15	Profiles of Intact Mitochondria	0.22 [0.18 – 0.72]	0.33 [0.16 – 0.49]	0.971
	Profiles of Disturbed Mitochondria	4.36 [1.19 – 5.83]	4.22 [1.51 – 7.63]	0.641

	Volume Density of Intact Mitochondria	0.37 [0.22 – 0.92]	0.43 [0.28 – 0.56]	0.858
	Volume Density of Disturbed Mitochondria	2.13 [1.06 – 4.66]	3.91 [1.26 – 7.06]	0.449
	Surface-to-Volume Ratio of the Inner Mitochondrial Membrane	0.90 [0.68 – 1.05]	0.99 [0.87 – 1.15]	0.302

198

Table e4. Comparison of Mitochondrial Morphology between Day 5 and 15 only including Patients that were investigated on both Days

Variables	Day 5	Day 15	p-value
Profiles of Intact Mitochondria	0.24 [0.19 – 0.81]	0.28 [0.18 – 0.60]	0.177
Profiles of Disturbed Mitochondria	3.83 [1.19 – 6.60]	3.89 [1.19 – 5.76]	0.532
Volume Density of Intact Mitochondria	0.41 [0.30 – 0.92]	0.37 [0.25 – 0.88]	0.691
Volume Density of Disturbed Mitochondria	2.90 [0.90 – 5.67]	2.13 [1.06 – 4.60]	0.211
Surface-to-Volume Ratio of the Inner Mitochondrial Membrane	0.77 [0.47 – 0.99]	0.90 [0.81 – 1.07]	0.363

203 **Table e5. Primer pairs for quantitative RT-PCR**

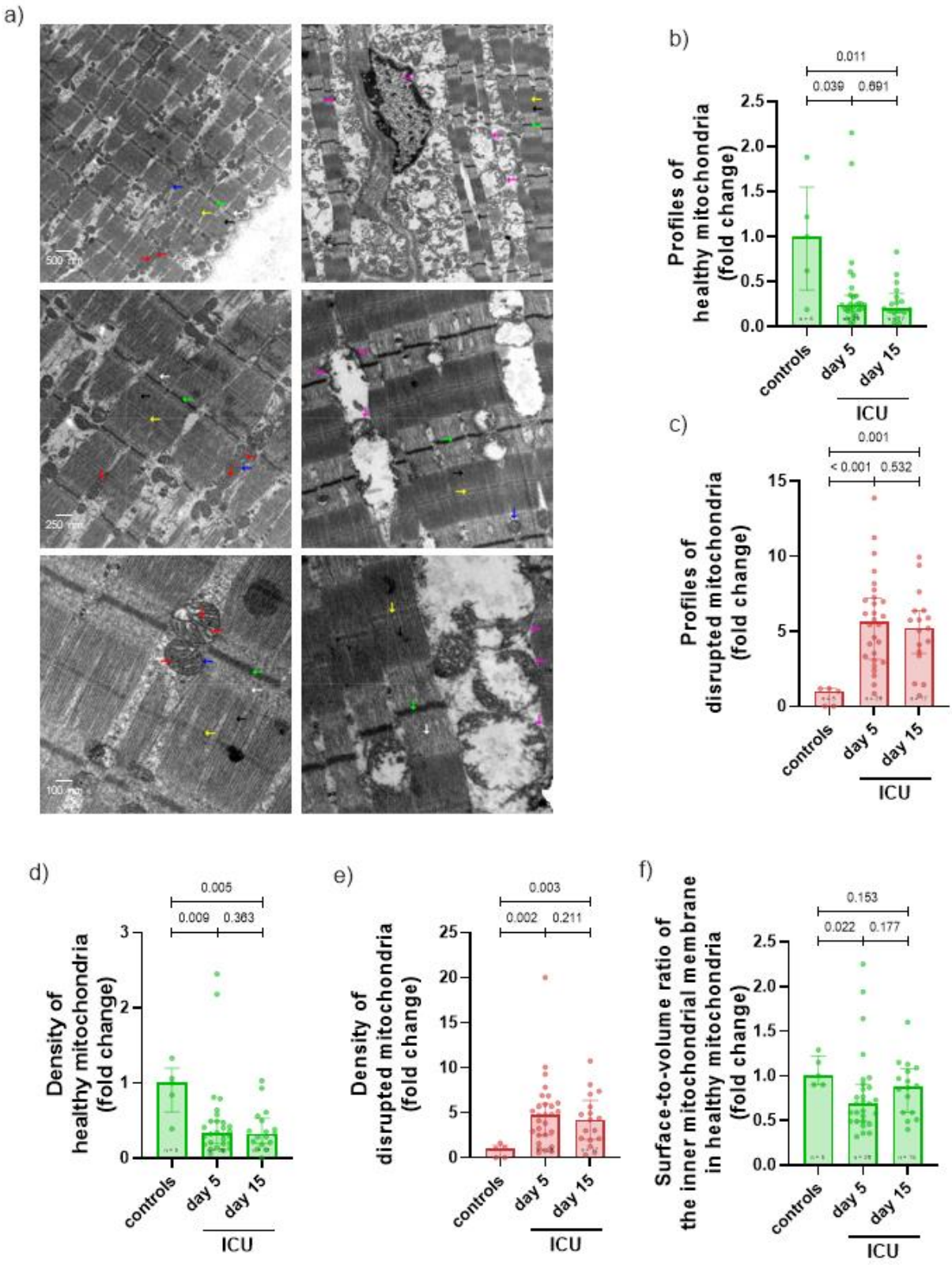
Gene	**Sequence (5´- 3´)**
Hs_*GAPDH* forward	GAAGGTGAAGGTCGGAGTCA
Hs_*GAPDH* reverse	AATGAAGGGGTCATTGATGG
Hs_*NDUFB8* forward	GAAGACTACGAACCTTACCCG
Hs_*NDUFB8* reverse	GTTCACCCCAGTTCAACCTC
Hs_*SDHB* forward	GACAAGGCTGGAGACAAAC
Hs_*SDHB* reverse	CGGAAGGTCAAAGTAGAGTCA
Hs_*UQCRC2* forward	CTGCGTCTTACATCCAGTCTG
Hs_*UQCRC2* reverse	GCGGTCACACTTAATTTGCC
Hs_*COX4* forward	GCCATGTTCTTCATCGGTTT
Hs_*COX4* reverse	CAAACAGAGCCCAAGGTGAC
Hs_*ATP5A1* forward	TGGGCGTGTCTTAAGTATTGG
Hs_*ATP5A1* reverse	TGTCAGGTTCCAAGTTCAAGG
Hs_*PPARGC1B* forward	GAGACGCTCTATCATGCACC
Hs_*PPARGC1B* reverse	TTGATGTTGGGTAGGATGTGG
Hs_*PPARA* forward	GCTATCATTACGGAGTCCACG
Hs_*PPARA* reverse	TCGCACTTGTCATACACCAG
Hs_*PPARG* forward	CTCCTATTGACCCAGAAAGCG
Hs_*PPARG* reverse	GAGTGGTCTTCCATTACGGAG
CytB	Hs02596867_s1 MT-CyB
MTCO1	Hs02596864_g1 MT-Co1
NRF-1	Hs00602161_m1
TFAM	Hs00273372_s1

204

ATP5A1 indicates ATP synthase subunit alpha; *COX4*, cytochrome c oxidase subunit 4, mitochondrial; *CYTB*, mitochondrial encoded cytochrome b; *GAPDH*, Glyceraldehyde 3-phosphate dehydrogenase; *MTCO1*, cytochrome c oxidase subunit 1; NRF1, nuclear respiratory factor 1; *NDUFB8*, NADH:ubiquinone oxidoreductase subunit B8; *PPARGC1A*, peroxisome proliferator-activated receptor gamma coactivator 1-alpha; *PPARGC1B*, peroxisome proliferator-activated receptor gamma coactivator 1-beta; *PPARA*, peroxisome proliferator-activated receptor alpha; *PPARG*, peroxisome proliferator-activated receptor gamma; *SDHB*, succinate dehydrogenase complex iron sulfur subunit B; *TFAM*, transcription factor A, mitochondrial; *UQCRC2*, cytochrome b-c1 complex subunit 2, mitochondria.

eFigures

Figure e1. Mitochondrial ultrastructure is disturbed in skeletal muscle of ICU patients.

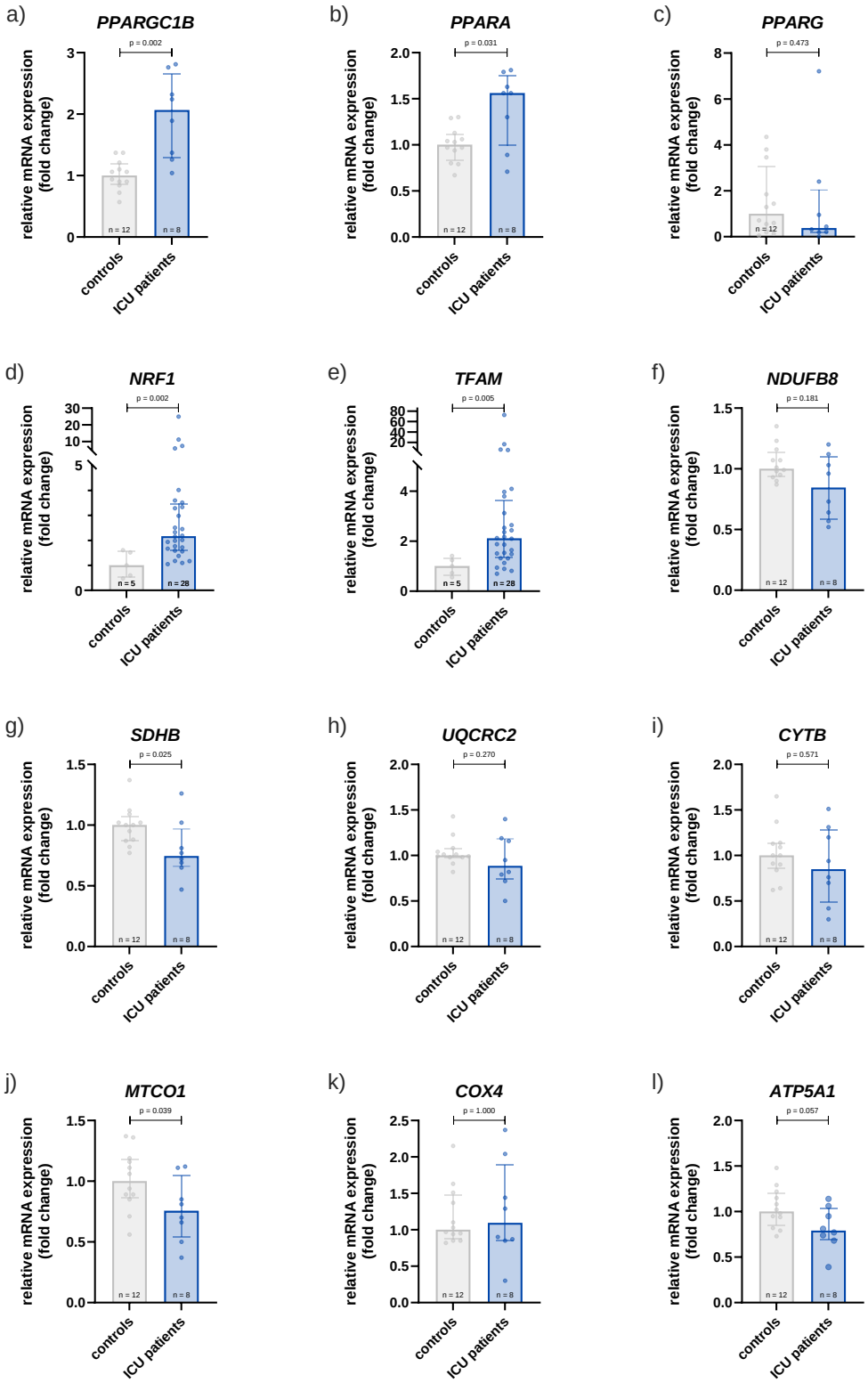


a) Representative transmission electron microscopy images from skeletal muscle biopsy specimens of control and ICU patients. (left colum; increasing magnification from top to bottom panel) Representative electron micrographs from critically ill patients showing macroscopically unremarkable mitochondria (blue arrow) with intact membrane structures of the outer as well as inner membrane (red arrow) in between sarcomeres (yellow arrow = M-band; green arrow = Z-disc; white arrow = I-band and black arrow = A-band). Mitochondria displayed here were classified as intact. Scale bars are indicated. (right colum; increasing magnification from top to bottom panel) Representative electron micrographs from critically ill patients showing swollen and destroyed mitochondria (pink arrow) with discontinuous membrane structures of the outer and inner membrane in between sarcomeres (yellow arrow = M-band; green arrow = Z-disc; white arrow = I-band and black arrow = A-band). Scale bars are indicated.

Analyses of the number of profiles of b) intact (median [IQR] of fold change; controls: 1.00 [0.62 – 1.22]; ICU day 5: 0.24 [0.18 – 0.34], p = 0.039 vs. controls; ICU day 15: 0.20 [0.16 – 0.33], p = 0.011 vs. controls; p = 0.691 ICU day 5 vs ICU day 15) and c) disturbed (median [IQR] of fold change, controls: 1.00 [0.00- 1.18], ICU day 5: 5.62 [3.20 – 7.17], p < 0.001 vs. controls; ICU day 15: 5.20 [3.67 – 6.36], p = 0.001 vs. controls; p = 0.532 ICU day 5 vs ICU day 15) mitochondria, volume density of d) intact (median [IQR] of fold change; controls: 1.00 [0.84 – 1.06]; ICU day 5: 0.33 [0.20 – 0.49], p = 0.009 vs. controls; day 15: 0.32 [0.21 – 0.50], p = 0.005 vs. controls; p = 0.363 ICU day 5 vs. ICU day 15) and e) disturbed (median [IQR] of fold change, controls: 1.00 [0.00 – 1.11], ICU day 5: 4.76 [2.53 – 5.99], p = 0.002 vs. controls; ICU day 15: 4.21 [2.10 – 5.65], p = 0.003 vs. controls; p = 0.211 ICU day 5 vs. ICU day 15) mitochondria and the f) surface-to-volume ratio of the inner mitochondrial membrane of intact mitochondria (median [IQR] of fold change, controls: 1.00 [0.90- 1.15], ICU day 5: 0.69 [0.49 – 0.89], p = 0.022 vs. controls; ICU day 15: 0.88 [0.59 – 1.07], p = 0.153 vs. controls; p = 177 ICU day 5 vs. ICU day 15) are shown. Data are shown as median and interquartile range [IQR].

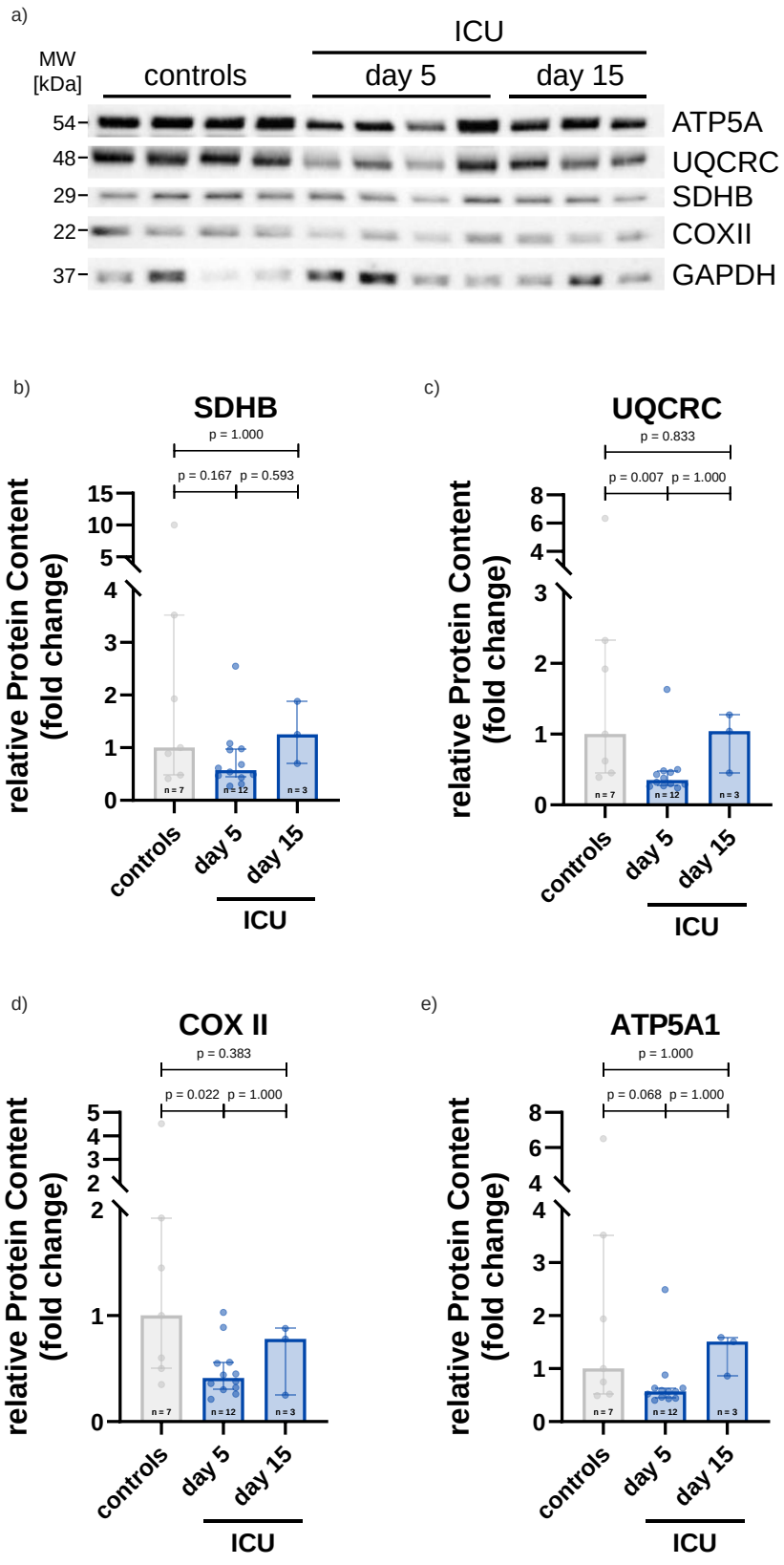
244 Statistical comparisons were performed with Mann-Whitney-U-Test for all comparisons versus
245 healthy controls, and Wilcoxon-signed rank-Test within ICU patients (day 15 vs day 5).

Figure e2. A dysregulation of mitochondrial genes and transcription factors occurs in muscle of ICU patients.



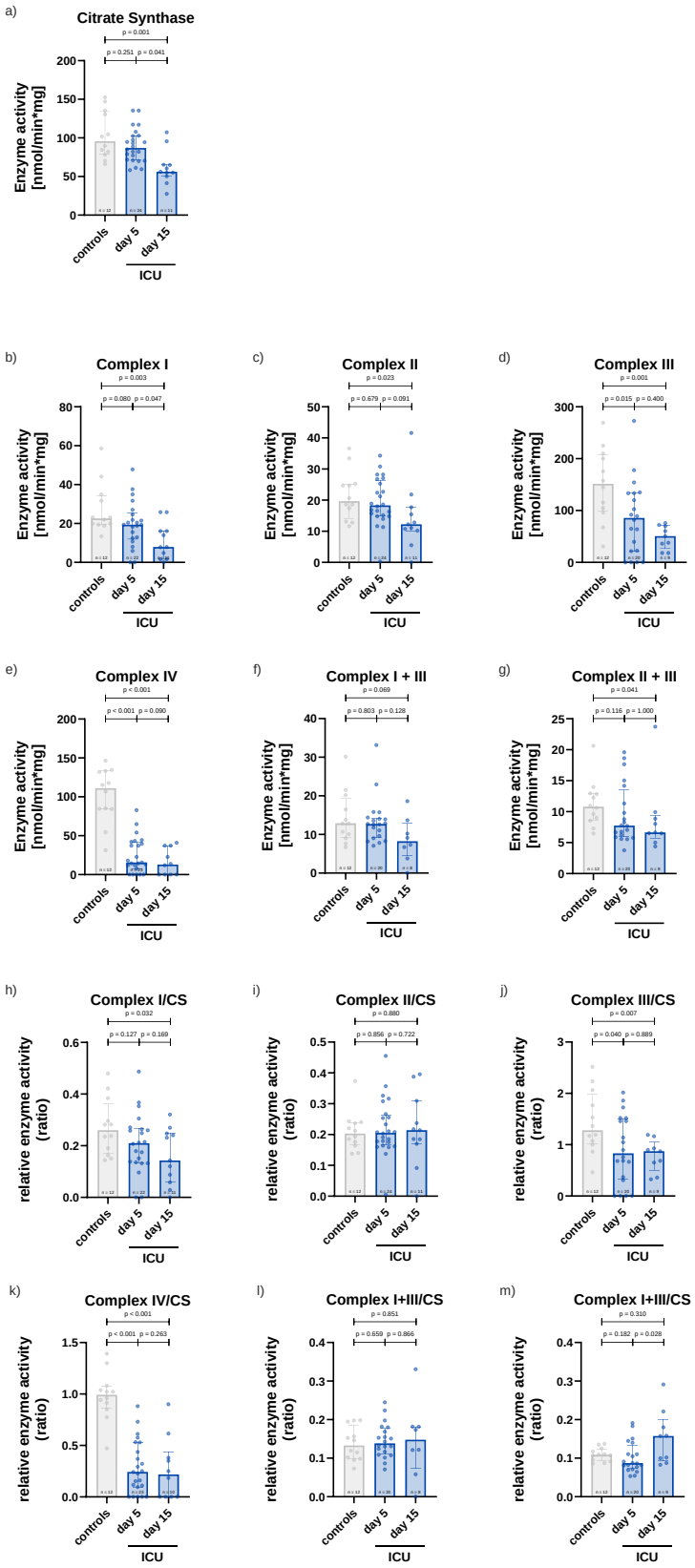
Quantitative RT-PCR of transcription factors for mitochondrial biogenesis (a) *PPARGC1B* (median [IQR] of a fold change –controls: 1.00 [0.87 – 1.15] vs. ICU patients 2.07 [1.31 – 2.54], p = 0.002), b) *PPARA* (median [IQR] of fold change, controls: 1.00 [0.87 – 1.10] vs. ICU patients 1.56 [1.10 – 1.71]; p = 0.031), c) *PPARG* (median [IQR] of fold change, controls: 1.00 [0.38 – 2.65] vs. ICU patients 0.38 [0.21 – 1.68], p = 0.473)*(ICU patients n = 8, sample size cannot be displayed within the figure as the bar graph is too shallow), d) NRF1* (median [IQR] of a fold change - controls: 1.00 [0.60 – 1.52] vs. ICU patients 2.17 [1.63 – 3.43], p = 0.002) *and e) TFAM* (median [IQR] of fold change, controls: 1.00 [0.73 – 1.24] vs. ICU patients 2.11 [1.40 – 3.46], p = 0.005)) and genes of electron transport complexes (f) *NDUFB8* (median [IQR] of fold change, controls: 1.00 [0.94 – 1.12] vs. ICU patients 0.85 [0.61 – 1.08], p = 0.181), g) *SDHB* (median [IQR] of fold change, controls: 1.00 [0.88 – 1.05] vs. ICU patients 0.74 [0.67 – 0.91], p = 0.025), h) *UQRCR2*, i) *CYTB*, j) *MTCO1* (median [IQR] of fold change, controls: 1.00 [0.87 – 1.18] vs. ICU patients 0.75 [0.58 – 0.99], p = 0.039), k) *COX4* (median [IQR] of fold change, controls: 1.00 [0.90 – 1.44] vs. ICU patients 1.10 [0.86 – 1.74], p = 1.000)*, l) ATP5A1* (median [IQR] of fold change, controls: 1.00 [0.88 – 1.18] vs. ICU patients 0.79 [0.71 – 1.00], p = 0.057)) in muscle of ICU patients and controls. *ATP5A1* indicates ATP synthase subunit alpha; *COX4*, Cytochrome c oxidase subunit 4; *CYTB*, mitochondrial encoded Cytochrome b; *MTCO1*, Cytochrome c oxidase subunit 1; *NDUFB8* indicates NADH:Ubiquinone Oxidoreductase Subunit B8; *NRF1*, Nuclear Respiratory Factor 1; *PPARA*, Peroxisome proliferator-activated receptor alpha; *PPARG*, Peroxisome proliferator-activated receptor gamma; *PPPARGC1B*, Peroxisome proliferator-activated receptor gamma coactivator 1-beta; *SDHB*, Succinate Dehydrogenase Complex Iron Sulfur Subunit B; *TFAM*, mitochondrial Transcription Factor A; *UQRCR2*, Cytochrome b-c1 complex subunit 2, mitochondria. Data are presented as median and interquartile range. Statistical comparisons were performed with Mann-Whitney-U-Test for all comparisons versus healthy controls, and Wilcoxon-signed rank-Test within ICU patients (day 15 vs day 5).

Figure e3. The content of ETC proteins is reduced in skeletal muscle of ICU patients.



a) Representative Western blot analyses of protein lysates from *vastus lateralis* of control and ICU with the anti OXPHOS-antibody detecting b) SDHB (median [IQR] of fold change, controls: 1.00 [0.68 – 2.73]; day 5: 0.58 [0.45 – 0.97], p = 0.167 vs. controls; day 15: 1.25 [0.97 – 1.57], p = 1.000 vs. controls; p = 0.593 for comparison between day 5 and day 15), c) UQCRC2 (median [IQR] of fold change, controls: 1.00 [0.54 – 2.21]; day 5: 0.35 [0.28 – 0.47], p = 0.007 vs. controls; day 15: 1.04 [0.74 – 1.15], p = 0.833 vs. controls; p = 1.000 for comparison between day 5 and day 15), d) COXII (median [IQR] of fold change, controls: 1.00 [0.55 – 1.69]; day 5: 0.41 [0.31 – 0.56], p = 0.022 vs. controls; day 15: 0.78 [0.52 – 0.83], p = 0.383 vs. controls; p = 1.000 for comparison between day 5 and day 15), and e) ATP5A1 (median [IQR] of fold change, controls: 1.00 [0.633 – 2.73]; day 5: 0.57 [0.45 – 0.63], p = 0.068 vs. controls; day 15: 1.51 [1.19 – 1.55], p = 1.000 vs. controls; p = 1.000 for comparison between day 5 and day 15) are shown. GAPDH was used as loading control. b-e) Quantification of Western blot signals from A. ATP5A1 indicates ATP synthase subunit alpha; COXII, Cytochrome c oxidase subunit 2; SDHB, Succinate Dehydrogenase Complex Iron Sulfur Subunit B; UQCRC2, Cytochrome b-c2 complex. Data are presented as median and interquartile range. Statistical comparisons were performed with Mann-Whitney-U-Test for all comparisons versus healthy controls, and Wilcoxon-signed rank-Test within ICU patients (day 15 vs day 5).

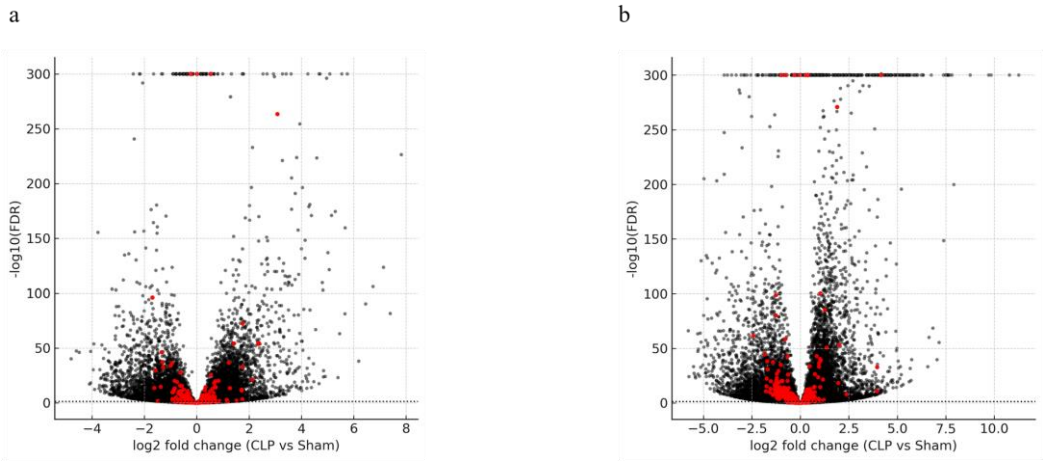
Figure e4. Mitochondrial function is decreased in skeletal muscle of ICU patients.



298 a-m) Spectrophotometric analyses of electron transport complexes (ETC) enzyme activities of
299 citrate synthase (median [IQR] of activity, controls: 95.6 [80.1 – 133.0]; day 5: 87.0 [71.4 –
300 102.7], p = 0.251 vs. controls; day 15: 56.3 [52.7 – 65.1], p = 0.001 vs. controls; p = 0.041 for
301 comparison between day 5 and day 15), complex I (median [IQR] activity, controls: 22.6 [19.6
302 – 33.3]; day 5: 19.4 [12.5 – 24.6], p = 0.080 vs. controls; day 15: 7.9 [3.2 – 16.1], p = 0.003 vs.
303 controls; p = 0.047 for comparison between day 5 and day 15) (median [IQR] ratio, controls:
304 0.26 [0.18 – 0.34]; day 5: 0.21 [0.14 – 0.26], p = 0.127 vs. controls; day 15: 0.14 [0.07 – 0.24],
305 p = 0.032 vs. controls; p = 0.169 for comparison between day 5 and day 15), II (median [IQR]
306 activity, controls: 19.6 [15.3 – 25.0]; day 5: 18.3 [15.0 – 26.0], p = 0.679 vs. controls; day 15:
307 12.2 [10.5 – 16.6], p = 0.023 vs. controls; p = 0.091 for comparison between day 5 and day
308 15)(median [IQR] ratio, controls: 0.20 [0.17 – 0.24]; day 5: 0.21 [0.17 – 0.26], p = 0.856 vs.
309 controls; day 15: 0.21 [0.18 – 0.27], p = 0.880 vs. controls; p = 0.722 for comparison between
310 day 5 and day 15), III (median [IQR] activity, controls: 151.4 [100.5 – 205.0]; day 5: 85.6 [22.1
311 – 133.3], p = 0.015 vs. controls; day 15: 50.5 [36.0 – 69.8] p = 0.001 vs. controls; p = 0.400 for
312 comparison between day 5 and day 15) (median [IQR] ratio, controls: 1.28 [1.00 – 1.91]; day
313 5: 0.83 [0.34 – 1.49], p = 0.040 vs. controls; day 15: 0.87 [0.65 – 0.93], p = 0.007 vs. controls;
314 p = 0.889 for comparison between day 5 and day 15), IV (median [IQR] activity, controls: 111.2
315 [84.4 – 132.7]; day 5: 15.6 [9.9 – 40.8], p < 0.001 vs. controls; day 15: 12.9 [0.0 – 37.2], p <
316 0.001 vs. controls; p = 0.090 for comparison between day 5 and day 15)(median [IQR] ratio,
317 controls: 0.99 [0.88 – 1.06]; day 5: 0.24 [0.10 – 0.48], p < 0.001 vs. controls; day 15: 0.22 [0.00
318 – 0.38], p < 0.001 vs. controls; p = 0.263 for comparison between day 5 and day 15), I+III
319 (median [IQR] activity, controls: 12.9 [9.6 – 18.3]; day 5: 12.7 [9.3 – 14.2], p = 0.803 vs.
320 controls; day 15: 8.2 [5.3 – 12.0], p = 0.069 vs. controls; p = 0.128 for comparison between day
321 5 and day 15)(median [IQR] ratio, controls: 0.13 [0.10 – 0.18]; day 5: 0.14 [0.11 – 0.17], p =
322 0.659 vs. controls; day 15: 0.15 [0.09 – 0.18], p = 0.851 vs. controls; p = 0.866 for comparison
323 between day 5 and day 15), II+III (median [IQR] activity, controls: 10.8 [8.8 – 12.9]; day 5: 7.7

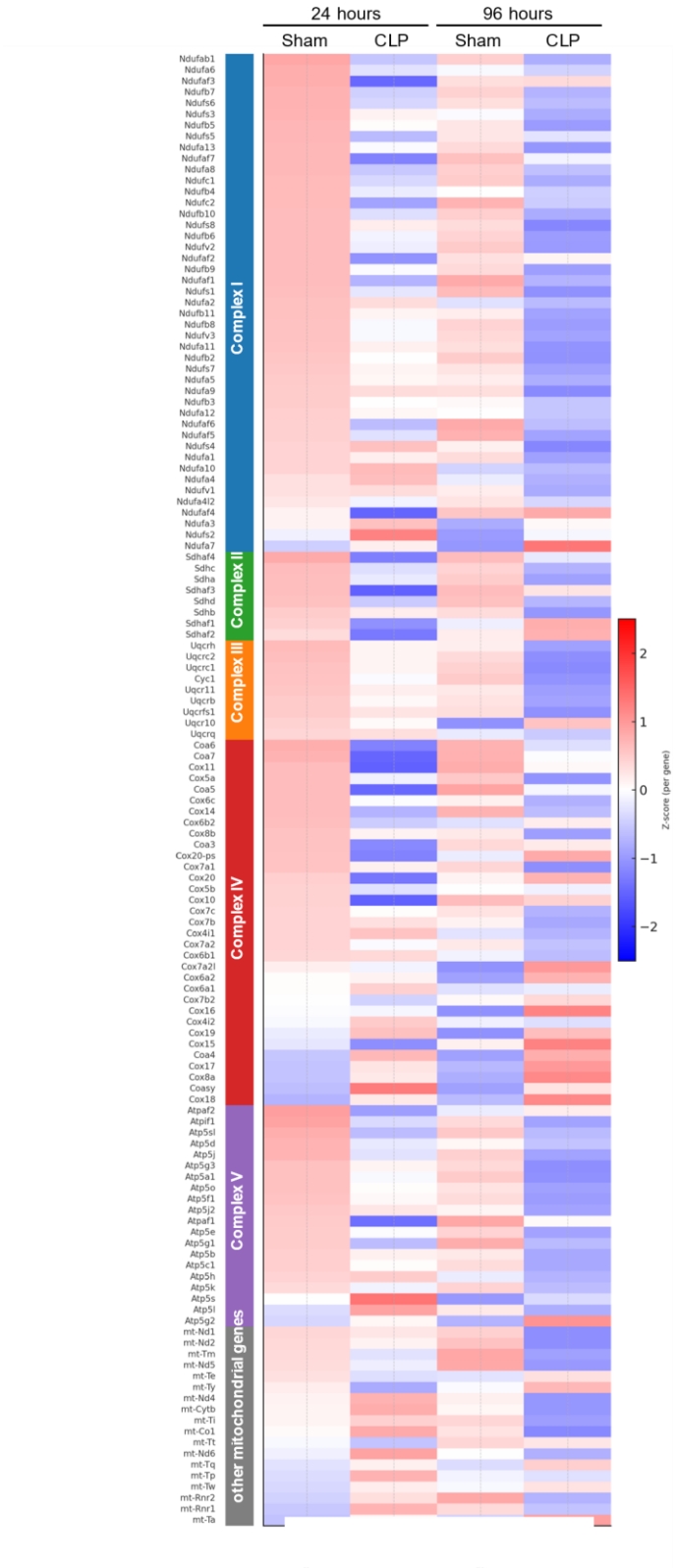
[6.1 – 12.8], p = 0.116 vs. controls; day 15: 6.6 [6.5 – 8.9], p = 0.041 vs. controls; p = 1.000 for comparison between day 5 and day 15)(median [IQR] ratio, controls: 0.11 [0.09 – 0.12]; day 5: 0.09 [0.07 – 0.13], p = 0.182 vs. controls; day 15: 0.16 [0.10 – 0.18], p = 0.310 vs. controls; p = 0.028 for comparison between day 5 and day 15) and V in muscle protein lysates of ICU patients after 5 and 15 days in ICU compared to controls. Enzyme activities are presented as enzyme activity per tissue wet-weight (nmol/min*mg; a-g) and related to CS-activity as ratio (h-m). Statistical comparisons were performed with Mann-Whitney-U-Test for all comparisons versus healthy controls, and Wilcoxon-signed rank-Test within ICU patients (day 15 vs day 5).

Figure e5. Volcano plots of differential gene expression in mouse tibialis anterior muscle following CLP-induced sepsis.



Volcano plots show log2 fold change (CLP vs sham) versus −log10(FDR) at (a) 24 hours and (b) 96 hours after surgery. The dotted black line denotes FDR = 0.05. All genes are shown as black circles, while mitochondrial-related genes (defined by curated mitochondrial gene sets including mtDNA-encoded OXPHOS subunits and nuclear-encoded mitochondrial genes) are shown as red circles.

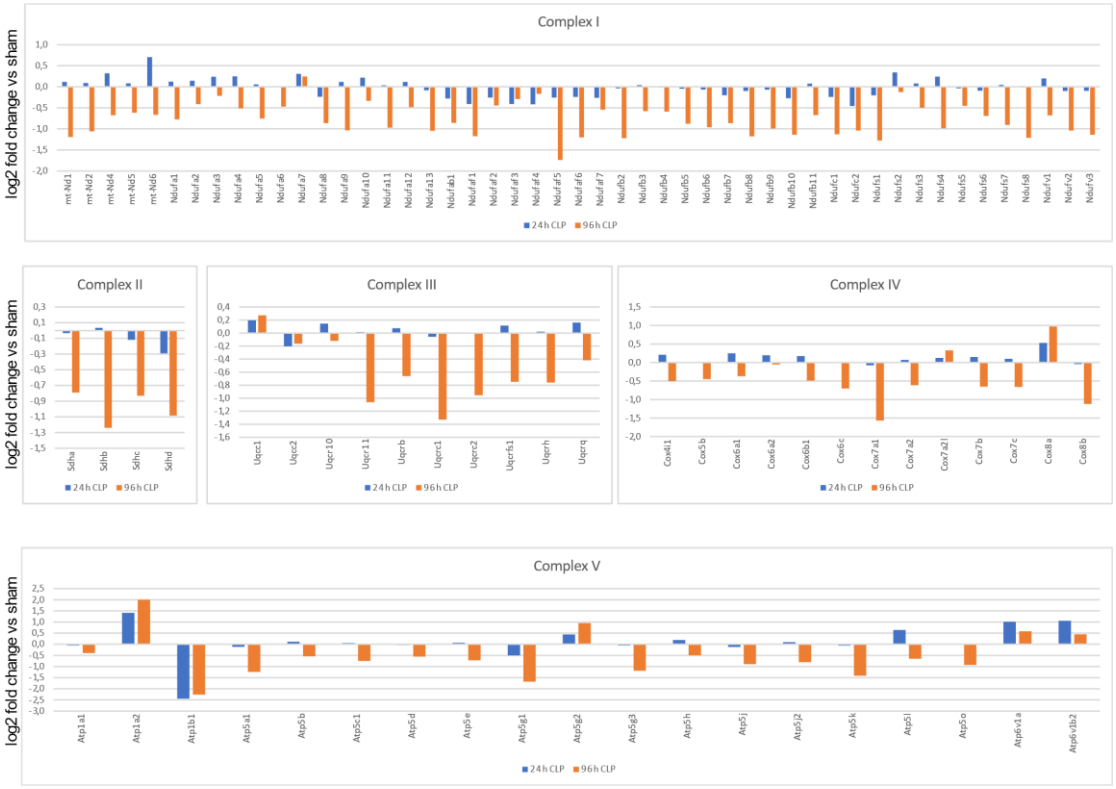
Figure e6. Mitochondrial gene expression organized by ETC complex.



Heat map of z-transformed log2-CPM expression (per gene) summarized as group means across 24h_Sham, 24h_CLP, 96h_Sham, and 96h_CLP. Genes are grouped by ETC Complex

348 I–V (color bar aligned to rows) with “other mitochondrial” genes shown below, and ordered
349 within each complex by variability in 24h_Shams.

Figure e7. Expression of mitochondrial genes contained in ETC complexes I-V in mouse TA muscle after 24 and 96 hours of sepsis.



WT mice were subjected to CLP or sham surgery. RNA sequencing analyses were performed 24 hours and 96 hours after surgery (WT Sham, n=6; WT CLP, n=6, for both time points). Expression of genes contained in electron transport chain (ETC) complexes I, II, III, IV, and V in tibialis anterior (TA) muscle of sham- and cecal ligation and puncture-operated mice after 24 hours and 96 hours. Only significantly up- or downregulated genes in at least one time point are shown (Log2 fold change, adjusted p-value < 0.05).

References

1. Rathke T. Erworbene Muskelschwäche auf der Intensivstation – Elektronenmikroskopisches Korrelat in der Frühphase der kritischen Erkrankung. 2016.

2. Reynolds ES. The use of lead citrate at high pH as an electron-opaque stain in electron microscopy. J Cell Biol. 1963;17(1):208-12.

3. Holzer MT, Uruha A, Roos A, Hentschel A, Schanzer A, Weis J, et al. Anti-Ku + myositis: an acquired inflammatory protein-aggregate myopathy. Acta Neuropathol. 2024;148(1):6.

4. Tschanz S, Schneider JP, Knudsen L. Design-based stereology: Planning, volumetry and sampling are crucial steps for a successful study. Ann Anat. 2014;196(1):3-11.

5. Tschanz SA, Burri PH, Weibel ER. A simple tool for stereological assessment of digital images: the STEPanizer. J Microsc. 2011;243(1):47-59.

6. Hsia CC, Hyde DM, Ochs M, Weibel ER, Structure AEJTFoQAoL. An official research policy statement of the American Thoracic Society/European Respiratory Society: standards for quantitative assessment of lung structure. Am J Respir Crit Care Med. 2010;181(4):394-418.

7. Nielsen J, Gejl KD, Hey-Mogensen M, Holmberg HC, Suetta C, Krustrup P, et al. Plasticity in mitochondrial cristae density allows metabolic capacity modulation in human skeletal muscle. J Physiol. 2017;595(9):2839-47.

8. Hahn A, Kny M, Pablo-Tortola C, Todiras M, Willenbrock M, Schmidt S, et al. Serum amyloid A1 mediates myotube atrophy via Toll-like receptors. J Cachexia Sarcopenia Muscle. 2020;11(1):103-19.

9. Wollersheim T, Grunow JJ, Carbon NM, Haas K, Malleike J, Ramme SF, et al. Muscle wasting and function after muscle activation and early protocol-based physiotherapy: an explorative trial. J Cachexia Sarcopenia Muscle. 2019;10(4):734-47.

10. Wollersheim T, Woehlecke J, Krebs M, Hamati J, Lodka D, Luther-Schroeder A, et al. Dynamics of myosin degradation in intensive care unit-acquired weakness during severe critical illness. Intensive Care Med. 2014;40(4):528-38.

11. Dobin A, Davis CA, Schlesinger F, Drenkow J, Zaleski C, Jha S, et al. STAR: ultrafast universal RNA-seq aligner. Bioinformatics. 2013;29(1):15-21.

12. Liao Y, Smyth GK, Shi W. featureCounts: an efficient general purpose program for assigning sequence reads to genomic features. Bioinformatics. 2014;30(7):923-30.

13. Love MI, Huber W, Anders S. Moderated estimation of fold change and dispersion for RNA-seq data with DESeq2. Genome Biol. 2014;15(12):550.

14. Huang da W, Sherman BT, Lempicki RA. Systematic and integrative analysis of large gene lists using DAVID bioinformatics resources. Nat Protoc. 2009;4(1):44-57.

15. Huang da W, Sherman BT, Lempicki RA. Bioinformatics enrichment tools: paths toward the comprehensive functional analysis of large gene lists. Nucleic Acids Res. 2009;37(1):1-13.

16. Zanders L, Kny M, Hahn A, Schmidt S, Wundersitz S, Todiras M, et al. Sepsis induces interleukin 6, gp130/JAK2/STAT3, and muscle wasting. J Cachexia Sarcopenia Muscle. 2022;13(1):713-27.

17. Wundersitz S, Pablo Tortola C, Schmidt S, Oliveira Vidal R, Kny M, Hahn A, et al. The Transcription Factor EB (TFEB) Sensitizes the Heart to Chronic Pressure Overload. Int J Mol Sci. 2022;23(11).

18. Grunow JJ, Reiher K, Carbon NM, Engelhardt LJ, Mai K, Koch S, et al. Muscular myostatin gene expression and plasma concentrations are decreased in critically ill patients. Crit Care. 2022;26(1):237.

19. Spinazzi M, Casarin A, Pertegato V, Salviati L, Angelini C. Assessment of mitochondrial respiratory chain enzymatic activities on tissues and cultured cells. Nat Protoc. 2012;7(6):1235-46.